Journal of Vibration Engineering & Technologies (2024) 12:5055–5071
https://doi.org/10.1007/s42417-023-01179-x

ORIGINAL PAPER

Real-Time Balancing and Position Tracking Control of 2-DOF Ball Balancer Using PID with Integral ANTI-WINDUP Controller

Basant Tomar[1] · **Narendra Kumar**[1] · **Mini Sreejeth**[1]

Received: 17 July 2023 / Revised: 5 October 2023 / Accepted: 8 October 2023 / Published online: 10 November 2023

Abstract

Purpose Ball balancer system is an electromechanical nonlinear system which has innate unstable and underactuated behaviour that can be helpful in realisation of both position tracking and balancing control problem in robotic systems analysis. This article presents the modelling, design, control and affirmation of 2-DOF ball balancer system. Different compensators are designed for specific transient and steady-state responses.

Methods The ball balancer system's model is developed in MATLAB Simulink, and the Quarc system is used for interfacing. Different compensators such as proportional–derivative (PD), proportional–integral–derivative (PID), PID with integral ANTI-WINDUP, with different velocity setpoints (V_{sw}) values along with different kind of inputs such as step input, ramp input and sinusoidal input are implemented over the 2D ball balancer system. After simulation, real-time experimentation is carried out on hardware setup. An overhead camera tracks the ball's position and controllers predict the precise position and provide the planar position of the ball as an output. The ball position, input voltage and plate angle comparisons are executed with different compensators for both simulation and real-time experimentation purposes.

Results The X–Y figures are obtained on scope with respect to different applied inputs and V_{sw} values. The closed loop responses show the signatures of the input servo motor voltage V_m(v), controlled output ball position x (cm) and servo load gear angle θ_l (degree). During simulation, PID compensator provides better results in terms of both transient and steady-state response. Step PD response with $V_{sw} = 0$ gives peak overshoot (PO%) as 5.62 and settling time as 2.39 s, whereas the step PID response with $V_{sw} = 0$, $\text{INTG}_{MAX} = 1.6$ deg and $T_{aw} = 0.001s$ gives peak overshoot (PO%) as 5.46 and settling time as 2.28 s. The steady-state error is also negligible in case of PID compensator. During real-time experimentation, for step PD response along x, e_{ss} is 0.61 cm which does not meet the requirements. But in case of PID step response, e_{ss} is 0.082 cm, which is hugely improved as compared to step PD response. PID square response is smoother than the PD square response. In addition, the trajectories of ramp PID responses is much smoother than the PD ramp responses. The outcomes of simulation and experimental assessment implies that PID compensator provides overall better control performances as compared to PD compensator for ball balancer system.

Conclusion The outcomes of simulation and experimental assessment implies that PID with integral ANTI-WINDUP controller has overall better control performances for ball balancer system. PID controller showed a better performance because of its ability to reduce the steady-state error that occurs between reference and generated output.

Keywords 2-DOF ball balancer system · Proportional–derivative (PD) controller · Proportional–integral–derivative (PID) with integral ANTI-WINDUP · Velocity setpoint

✉ Basant Tomar
basanttomar18@gmail.com

Narendra Kumar
narendrakumar@dtu.ac.in

Mini Sreejeth
minisreejeth@dce.ac.in

[1] Department of Electrical Engineering, Delhi Technological University, Delhi 110042, India

Introduction

The control theory evolution emphasises on methods of analytical controller design techniques, technological advancements and the implementation of these techniques in real time [1]. Control system is an area that correlates with diverse disciplines and approaches, which leads to the development of an automatic decision-making process that

improves the performance of control benchmark problems [2]. A significant area of control has been the management of autonomous robots performing difficult tasks in dynamic environments such as vehicle balancing [3, 4] and position control [5], trajectory tracking and path planning [6–8]. In the past, numerous attempts have been made to control autonomous robots. There are a number of control benchmark issues that are concerned with engineering systems like the inverted pendulum [9], the Furuta pendulum [10, 11], the beam and ball system [12], the hovercraft [13] and the ball and plate (B&P) system [14, 15].

The most prominent and well-known control benchmark application is the B&P system. It is used in robotic systems for balancing control and tracking position [16, 17]. The ball balancer system is an intrinsically unstable and nonlinear system having 2 degrees of freedom (DOF). In this arrangement, a ball slides on top of a plate that is attached on the output shaft of an electrical motor. By applying an electrically controlled signal, it is possible to balance the object about the axis of its centre of gravity. The nonlinear and underactuated behaviour of ball balancer systems significantly impacts the steady-state operation and position tracking.

The position tracking and balance control in robotic ball balancer systems is a widely researched problem because of its nonlinearity and instability. Generally, these systems find their application as benchmark systems for testing control laws and developing control strategies for problems related to the movement of robotic manipulators. Various controller architectures like fuzzy [18, 19], sliding mode [20, 21], linear quadratic control [22–24], PID controller [25] and metaheuristic techniques [26] have been used in the past for trajectory tracking, stabilisation and control of the ball balancer system.

Conventionally, classical controllers have made their way to be implemented with these systems. The proportional derivative and PID controllers both were applied with B&P system for the closed-loop system stability [27, 28]. Mohammadi et al. [29] applied a neural network-based feedback controller on B&P system in which two sub-controllers worked in parallel to reduce the dynamic errors in controller design. To eliminate coordinate transformation and minimise complexity, Zheng et al. [30] suggested a parallel thinning and window searching approach which used sensing camera for tracking the position and movement of the B&P system with both fuzzy and PID control. When the external disturbance is more intense, the main problem with conventional PID is that it cannot produce satisfactory eliminated outcomes. With differential feedback, these systems have a drawback that they cannot intensify measurement noises.

Similar to the forward-stepping controller, backstepping controller was proposed to generate a distinct control law for achieving better control performances more quickly [31]. Ma et al. [32] presented an observer integrated backstepping control technique for a cascaded B&P system which used a linear extended state observer and tracking differentiator to measure the uncertainties and derivatives of the virtual controls with Lyapunov theory. But these systems result in unwanted chattering entering the actuators of the system, harming both its mechanical and electronic components.

To adhere to all real-time requirements for position tracking and balance control, various studies have been conducted by the researchers in past. Elshamy et al. [33] proposed a hybrid pseudo-PD controller (fuzzy logic) for improving the stabilisation and tracking the trajectory of the B&P system which used different machine learning-based algorithms such as random forest, decision tree and support vector regression to detect the servo motor angle for correcting the ball plate position. While utilising the simplified model, some degree of control error is unavoidable.

Jang et al. [34] proposed an adaptive observer control technique based on virtual angle to solve the under-actuation problem without velocity measurements and local minima issue. It estimated the velocity information of robots with uncertainty using a neural network-based observer. Okafor et al. [35] developed a deep reinforcement learning-based PID controller for controlling and tracking the trajectory of a linearised B&P system, which used a customised deep deterministic policy gradient agent by altering the neural network architecture. But these systems do not guarantee the convergence of balancing and tracking errors.

Haddad et al. [36] presented a study by implementing different model-based controllers such as PID, LQR, linear model predictive control, state feedback control and linear quadratic tracker using ATmega328P microcontroller to control and stabilise a laboratory prototype of the B&P system. However, the greatest shortcoming with these traditional methods is the significant increase in peak overshoot and settling time. Fuzzy and sliding mode controllers have been widely discussed to overcome chattering phenomenon in a B&P system. Zaare et al. [37] implemented an adaptive fuzzy sliding mode controller based on state disturbance observer to control the position of ball and beam system with different uncertainties. A power reaching law-based radial basis function network adaptive control approach was proposed by Li et al. [38] to reduce the chattering problems of the ball balancer system. However, the high nonlinearities introduced by the pneumatic actuators overcomplicate the controller design.

Due to its intrinsic complexity, the ball balancer system has two key issues that must be resolved to sustain the ball in a precise spot and retain it there for reducing the tracking error as well as time. These issues involve controlling point stabilisation and balancing the ball on a plate. To address the issues raised above, this work focuses on

mathematical modelling, optimal parameter selection and constructing several controllers for the 2-DOF ball balancer system. Investigation and comparison of different control strategies used with a ball balancer were done. The major contributions of this research are summarised as follows.

(1) This work successfully simulates and implements different controllers including proportional–derivative (PD), proportional–integral–derivative (PID) and PID with Integral ANTI-WINDUP on a ball balancer system with different velocity setpoints (V_{sw}) values along with different inputs.
(2) The ball balancer system's model is developed in MATLAB Simulink and the Quarc system is used for interfacing.
(3) The compensators are designed for specific transient and steady-state responses.
(4) The ball position, input voltage and plate angle comparisons were executed with different compensators for both simulation and real-time experimentation purposes.

The article first focuses on modelling the 2-DOF ball balancer system, and then it turns to developing and implementing controllers for the setup using Simulink and real time. The findings for the ball balancer showed the impact of this innovative adaptation of the hybrid algorithm for optimising controllers. Finally, a simulation and experimentation comparison based on PD and PID controllers on a ball balancer is performed. This article is divided into the following sections. The ball balancer setup modelling and associated operational phenomena are described in the "2-DOF Ball Balancer System". Designing of various controllers for observing the plate's slope from the measurement of ball position is covered in "Designing Controllers for Ball Balancer System". To support the proposed technique, simulation results are shown along with the comparative analysis in "Results and Discussion", followed by the conclusion in the final section.

2-DOF Ball Balancer System

The 2DBB system is an electromechanical, second-order multi-input and multi-output system which is highly nonlinear and unstable [39]. 2DOFBB is the more sophisticated version of one DOF ball and beam system. The system's two inputs are servo input commands for the -*x* and *y*-axes, and its two outputs are the ball positions along the *x*- and - axes. To keep the system stable, it needs a feedback closed-loop controller.

The 2DoF ball balancer system addresses two control issues:

(a) Controlling the plate's inclination (i.e. the plate angle)
(b) Controlling the ball's position on the moving plate.

As the voltage is applied to the system, the rigid plate's slope changes, thus affecting the ball's movement as the plate's inclination changes. The servo motor's movement alters the plate's angle, which causes the ball to drop from

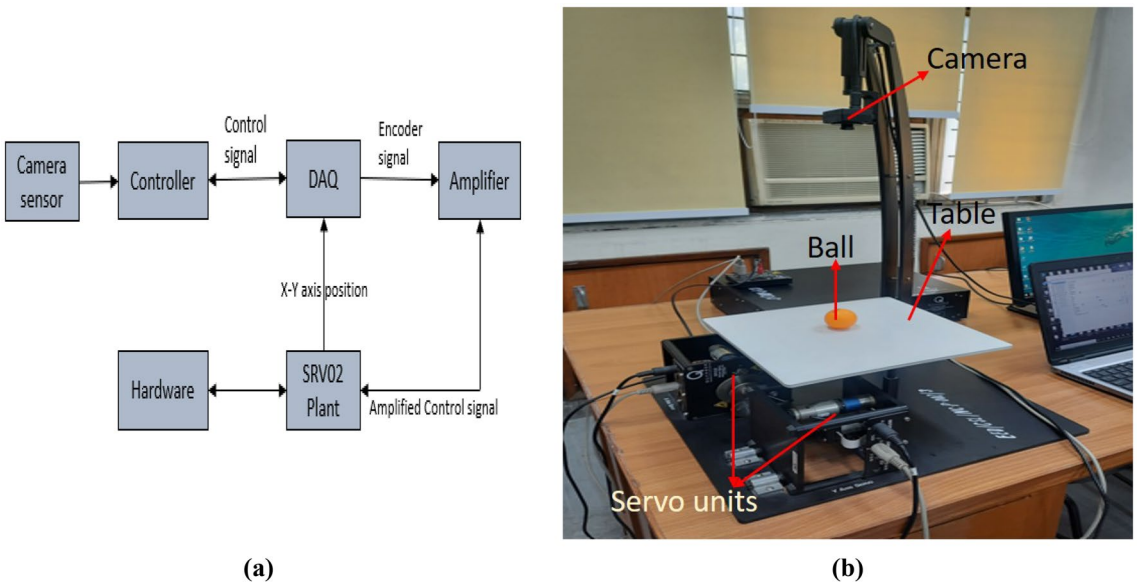

Fig. 1 **a** Block diagram of 2-DOF ball balancer system. **b** Hardware setup of 2DBB in laboratory

the plate [40]. Therefore, a controller is required with this system for balancing the ball movement on the plate.

Controller Design of the 2-DOF BB System

The real-time hardware model of the 2-DoF ball balancer system used for designing of Simulink model is manufactured by QUANSER [41]. A little plastic ball, two rotating servo motors, a power amplifier, a USB camera to record the image of ball location, a data gathering device, and a computer system with a feedback controller make up the hardware needed to conduct the experiment. A metallic plate with four quadrants is fixed to the 2-DOF ball balancer system with a gimbal joint in the middle that features a two-degree range of flexibility in rotation for tilting in the *x*- and *y*-axes. The two servo motors that are part of the 2DBB system are mechanically attached to the plate's axis and connected perpendicularly in the *x*- and *y*-directions. The two servo motors operate independently of one another [42]. The block diagram architecture of the B&P system is shown in Fig. 1a. The laboratory setup of the 2DoF B&P system's is depicted briefly in Fig. 1b.

Through the employment of a Faulhaber series DC micromotor, the plate rotates to balance the system in both directions [43]. This keeps the ball balanced on the metallic plate's quadrangular surface and prevents it from slipping off. The servo input voltage (SRV02) unit has a standard servo motor incorporated with a potentiometer, which is used to balance the ball in both axes. The standard control problem of this setup focusses mainly on balancing the ball on the square plate.

To obtain the ball movement with respect to voltage, a control signal, or plate inclination, is initially given to the data acquisition (DAQ) device from the hardware configuration, depicted in Fig. 1a. Using the Q2-USB data acquisition board, a longer period of time is spent in measuring the control signal related to the plate's disposition [49]. The information about the movement of the ball on the plate regarding the voltage change is provided by the measured signal. Additionally, the received signal is relayed to the controller along with the ball coordinates that were recorded using the camera. The controller performs the required steps to keep the ball balanced, and the DAQ repeats the process until the plate's stabilising angle is reached. The controller receives

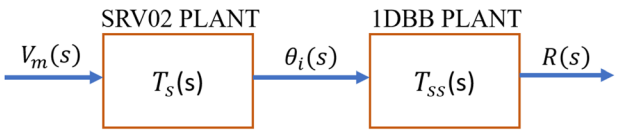

Fig. 3 Open-loop transfer function of the ball balancer system

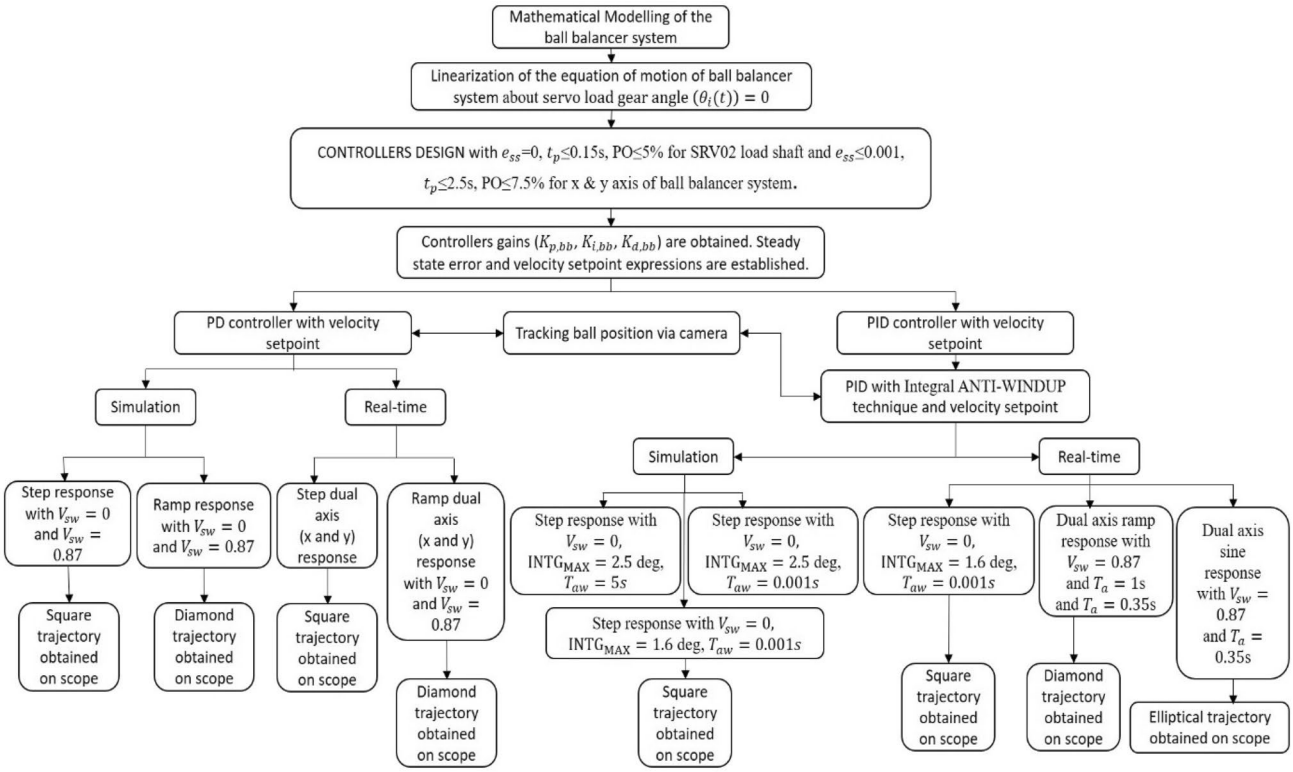

Fig. 2 Flowchart depicting the taxonomy of required steps used for balancing and position tracking control of the 2-DoF ball balancer system

signal from DAQ and then coordinates with the camera signal from the overhead camera with the help of a signal processing technique and then this controlled output signal is sent to the DAQ again, which delivers this encoded signal to the power amplifier for signal amplification. Then this amplified control signal is fed back to the hardware setup or SRV02 plant and this process repeats itself. The SRV02 plant unit, which is accomplished currently for position and balance control, may be implemented for further applications like vibrations and self-erecting controls in other setups suchas solar energy tracker, inverted pendulum, etc. which makes this system unit applications feasible and economical. Figure 2 displays a flowchart depicting the taxonomy of the required steps used for balancing and position tracking control of the 2-DoF ball balancer system.

Mathematical Modelling

Figure 3 displays the open-loop transfer function of the ball balancer system. The transfer function $T_s(s)$ represents the dynamics between the resulting load gear angle $\theta_i(s)$ and input servo motor voltage $V_m(s)$. The transfer function $T_{ss}(s)$ represents the dynamics between the position of the ball $R(s)$ and the servo load gear angle $\theta_i(s)$.

It is worthy to note that since this is a decoupled system in which the actuator dynamics of both are independent and will not affect each other, the SRV02 device is considered to be symmetrical for both the -x and y-axis. Therefore, modelling is represented only for a single axis. The block diagram of the 2D ball balancer's single axis (x-axis) is now shown as a 1D ball balancer (1DBB).

The complete transfer function ofthe 1DBB + SRV02 unit is:

$$T(s) = T_s(s)T_{ss}(s), \tag{1}$$

where the SRV02 transfer function is

$$T_s(s) = \theta_i(s)/V_m(s) \tag{2}$$

and 1DBB transfer function is

$$T_{ss}(s) = R(s)/\theta_i(s). \tag{3}$$

The equation of motion (eom) of the ball relative to the angle of beam (δ) will be of the form

$$\frac{d^2}{dt^2}x(t) = f(\delta(t)), \tag{4}$$

where $\delta(t)$ is a nonlinear function. The free body diagram (FBD) of the ball and plate system is shown in Fig. 4. The equation of motion can be used to determine how the ball moves with respect to the plate angle.

Neglecting both viscous damping and friction, the ball forces can be represented as:

$$\Sigma F = F_{x,t} - F_{x,r} = M_{\text{ball}}g, \tag{5}$$

$$\Sigma F = M_{\text{ball}}\left\{\frac{d^2}{dt^2}x(t)\right\}. \tag{6}$$

From FBD, when the inclination is positive, the force acting in the positive x-direction is

$$F_{x,t} = M_{\text{ball}}g\sin(\delta), F_{x,r} = \tau_{\text{ball}}/r_{\text{ball}}, \tag{7}$$

$$\tau_{\text{ball}} = J_{\text{ball}}\left\{\frac{d^2}{dt^2}\varnothing_{\text{ball}}(t)\right\}, \tag{8}$$

$$F_{x,r} = J_{\text{ball}}\left\{\frac{d^2}{dt^2}x(t)/{r_{\text{ball}}}^2\right\}, \tag{9}$$

where $F_{x,t}$ is the translational force due to gravity, $F_{x,r}$ is the ball's rotational inertia force,M_{ball} is the mass of the ball, δ is the beam angle, τ_{ball} is the ball torque, r_{ball} is the ball radius, $\varnothing_{\text{ball}}$ is the angle of ball and J_{ball} is the ball moment of inertia.

Substituting Eqs. (7) and (9) into Eq. (5),

$$\Sigma F = M_{\text{ball}}\left\{\frac{d^2}{dt^2}x(t)\right\} = M_{\text{ball}}g\sin(\delta) - J_{\text{ball}}\left\{\frac{d^2}{dt^2}x(t)/{r_{\text{ball}}}^2\right\}, \tag{10}$$

$$\frac{d^2}{dt^2}x(t) = M_{\text{ball}}g\sin(\delta){r_{\text{ball}}}^2/M_{\text{ball}}.{r_{\text{ball}}}^2 + J_{\text{ball}}. \tag{11}$$

The above Eq. (11) gives the final ball and plate system equation of motion. It is quite difficult to design a stabilising controller for the nonlinear system model. So, it is important to linearise the nonlinear system about a desired operating point to analyse the system behaviour such as stability, reference tracking, etc. In this work, Eq. (11) is linearised

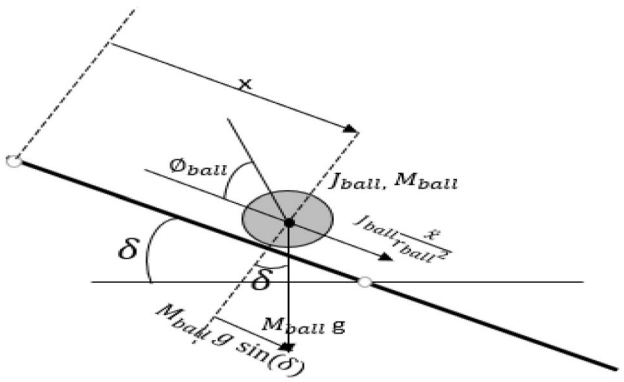

Fig. 4 FBD of the ball and plate system

about the servo load gear angle $\left(\theta_i(t)\right) = 0$ to use the model for Laplace-based PID controller design.

Inclusion of SRV02 Dynamics

Now, the ball position with respect to the servo load gear angle (θ_i) is to be obtained. The obtained equation of motion will be nonlinear in nature.

Considering the length of the plate to be L_p and the servo angle required to shift the beam height by 'H',

$$\sin(\delta(t)) = 2H/L_p, \sin(\theta_i(t)) = H/R_{\text{arm}}, \tag{12}$$

so the relation between the beam angle (δ) and servo load gear angle $\left(\theta_i\right)$ is

$$\sin(\delta(t)) = 2\sin(\theta_i(t))R_{\text{arm}}/L_p, \tag{13}$$

where R_{arm} is the arm radius.

Now, linearising Eq. (11) about the servo load gear angle $\left(\theta_i(t)\right) = 0$,

$$\frac{d^2}{dt^2}x(t) = \frac{2M_{\text{ball}}g\sin(\theta_i(t))R_{\text{arm}}{r_{\text{ball}}}^2}{(M_{\text{ball}}.{r_{\text{ball}}}^2 + J_{\text{ball}})L_p}. \tag{14}$$

At $\left(\theta_i(t)\right) = 0, \sin(\theta_i(t) = \theta_i(t)$.

By approximating the value, the linear equation of motion for the 1DBB plant is formulated as

$$\frac{d^2}{dt^2}x(t) = \frac{[2M_{\text{ball}}g.\theta_i(t)R_{\text{arm}}{r_{\text{ball}}}^2}{(M_{\text{ball}}.{r_{\text{ball}}}^2 + J_{\text{ball}})L_p}. \tag{15}$$

Equation (14) is a nonlinear equation as discussed above and Eq. (15) represents the linear equation of motion for the 1DBB plant. Lumping the coefficient parameters of $\theta_i(t)$ to get the parameter model gain (K_{m}) of the 1DBB system,

$$K_{\text{m}} = \frac{[2M_{\text{ball}}g.R_{\text{arm}}]{r_{\text{ball}}}^2}{(M_{\text{ball}}.{r_{\text{ball}}}^2 + J_{\text{ball}})L_p}. \tag{16}$$

So, the final linear equation of motion for the 1DBB plant becomes

$$\frac{d^2}{dt^2}x(t) = K_{\text{m}}.\theta_i(t). \tag{17}$$

Assume all initial conditions to be zero to get the transfer function $T_{\text{ss}}(s)$ for the 1DBB plant.

The Laplace transform of Eq. (17) will be

$$s^2X(s) - D(x(0)) - sx(0) = K_{\text{m}}.\theta_i(s), \tag{18}$$

$$X(s) = K_{\text{bb}}\theta_i(s)/s^2, T_{\text{ss}}(s) = K_{\text{m}}/s^2, \tag{19}$$

where K_{m} is the model gain.

The SRVO2 voltage to load angle transfer function is of type

$$T_{\text{s}}(s) = K/s(1 + \tau s). \tag{20}$$

So, the complete process becomes

$$T(s) = K\frac{K_{\text{m}}}{s^3(1 + \tau s)}, R(s) = V_m k\frac{K_{\text{m}}}{s^3(1 + \tau s)}. \tag{21}$$

Designing Controllers for the Ball Balancer System

The cascade control for the x-axis of the SRV02 + 2DBB system is depicted in the Fig. 5. 2DBB is a decoupled system. So, the x-axis actuator will not affect the response of the y-axis response. The SRV02 device is considered to be symmetrical for both the x- and y-axis. Therefore, modelling

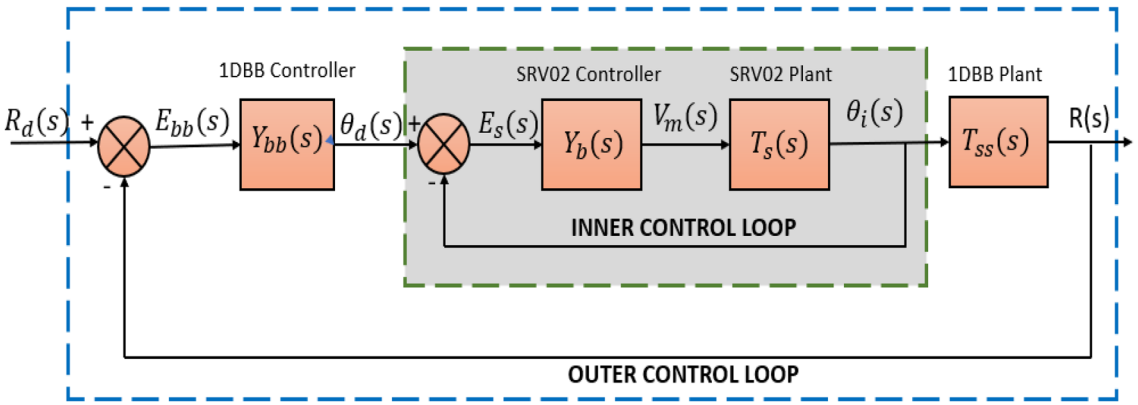

Fig. 5 Cascade control for the x-axis of the SRV02 + 2DBB system

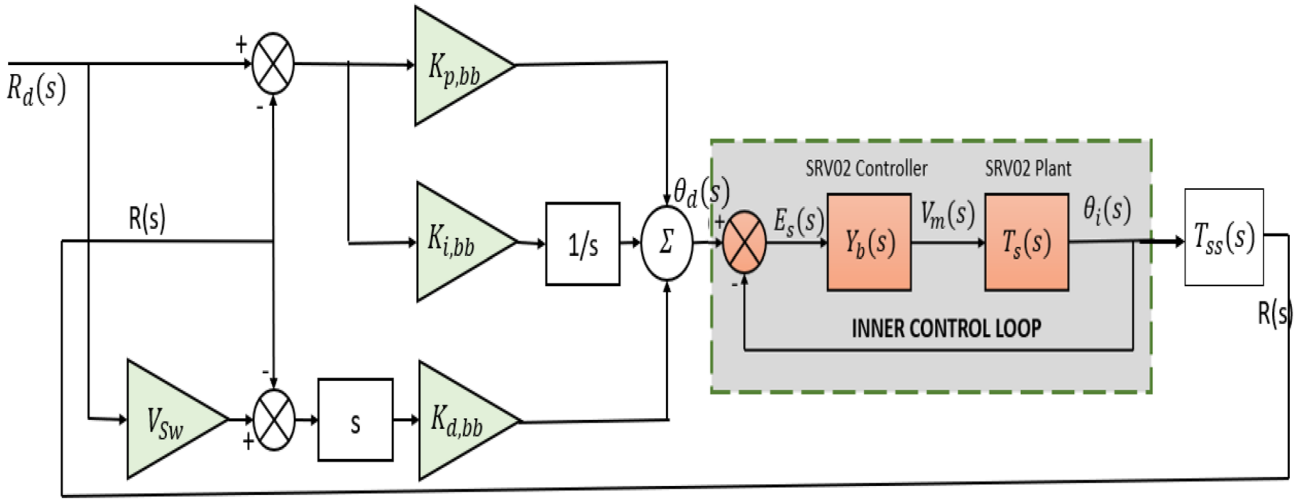

Fig. 6 Overall architecture of the proposed PID compensator

is represented only for the single axis. 2DBB single axis (x-axis) is represented as 1DBB.

Depending upon the ball position $R(s)$, the required servo load angle $\theta_{\mathrm{d}}(s)$ is computed by the ball balancer compensator $Y_{\mathrm{bb}}(s)$ to get the desired ball position $R_{\mathrm{d}}(s)$. Servo position control is described by the inner loop where the required motor voltage $V_{\mathrm{m}}(s)$ for the desired load angle is calculated by the servo compensator $Y_{\mathrm{b}}(s)$ and later on the compensator for the outer loop is designed.

For designing, it is desired to have the following criteria: e_{ss}=0, $t_p \leq 0.15$ s, PO ≤ 5% for SRV02 load shaft and $e_{\mathrm{ss}} \leq 0.001$, $t_p \leq 2.5$ s, PO ≤ 7.5% for the x- and y-axis of the ball balancer system, where, e_{ss} is steady − state error, t_p is peak time and PO is the peak overshoot.

For designing the inner control loop, the proportional-velocity (PV) controller gains are obtained when SRV02 is in high-gear configuration. The nominal SRV02 model parameters are $K = 1.78$ (rad/sV) and τ=0.0288 s, where K is steady-state gain and τ is time constant. To meet the above specifications, the desired damping ratio is 0.693 and minimum natural frequency is 28.82 (rad/s). Using nominal model parameters, the proportional control gain (K_{p}) is 13.57 (V/rad) and velocity control gain (K_{v}) is 0.0788 (Vs/rad). The outer control loop controls the ball position along the x-axis.

PID Control Design

The PID compensator, shown in Fig. 6, in time domain for the outer control loop is provided as:

$$\theta_{\mathrm{d}}(t) = K_{\mathrm{p,bb}}\{r_d(t) - r(t)\} + K_{\mathrm{d,bb}}\left[V_{\mathrm{sw}}\left\{\frac{d}{dt}r_{\mathrm{d}}(t)\right\} - \frac{d}{dt}r(t)\right] + K_{\mathrm{i,bb}}\int \left(r_{\mathrm{d}}(t) - r(t)\right)dt, \tag{22}$$

where θ_d is the required servo load angle, $K_{\mathrm{p,bb}}$ is the gain of proportional control action, $K_{\mathrm{i,bb}}$ is the gain of integral control action, $K_{\mathrm{d,bb}}$ is the derivative control action and V_{sw} represents the velocity setpoint weight.

With no servo dynamics, the outer-loop controller in Laplace domain is

$$\theta_{\mathrm{d}}(s) = \{K_{\mathrm{p,bb}} + K_{\mathrm{i,bb}}/s\}(R_d(s) - R(s)) + K_{\mathrm{d,bb}}s(V_{\mathrm{sw}}R_d(s) - R(s)). \tag{23}$$

As there is no servo dynamics, $\theta_d(s) = \theta_i(s)$, the control loop equation is

$$\frac{R(s)}{R_{\mathrm{d}}(s)} = \frac{K_{\mathrm{m}}\left(s^2K_{\mathrm{d,bb}}V_{\mathrm{sw}} + sK_{\mathrm{p,bb}} + K_{\mathrm{i,bb}}\right)}{s^3 + s^2K_{\mathrm{m}}K_{\mathrm{d,bb}} + sK_{\mathrm{m}}K_{\mathrm{p,bb}} + K_{\mathrm{m}}K_{\mathrm{i,bb}}}. \tag{24}$$

The prototype third-order characteristic equation is

$$(s^2 + 2\zeta\omega_n s + {\omega_n}^2)(s + a_0), \tag{25}$$

Table 1 PD and PID controller gains and parameters

Controllers	Pole location, a_0 (rad/s)	Steady-state gain, k (rad/Vs)	Time constant, τ (s)	V_{sw}	$K_{\mathrm{p,bb}}$ (rad/m)	$K_{\mathrm{i,bb}}$ (rad/sm)	$K_{\mathrm{d,bb}}$ (rad s/m)
PD	0	8.837	0.051	0	3.72	0	2.148
PID	1	8.837	0.051	0–1	5.819	3.693	2.967

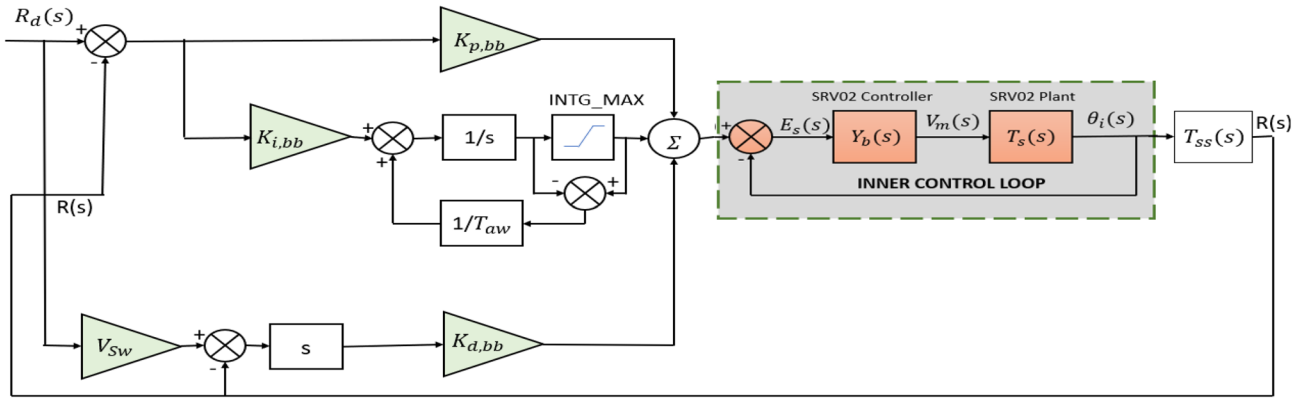

Fig. 7 PID compensator with Integral ANTI-WINDUP

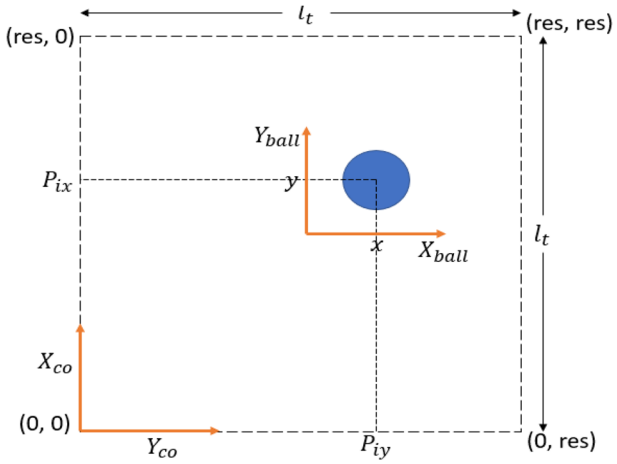

Fig. 8 Raw camera measurement of the ball position

$$s^3 + \left(2\zeta\omega_n + a_0\right)s^2 + \left(2\zeta\omega_n a_0 + {\omega_n}^2\right)s + ({\omega_n}^2 + a_0). \quad (26)$$

Comparing the characteristic Eqs. (24) and (26), the PID control action gains are formulated as

$$K_{\mathrm{p,bb}} = \frac{\omega_n\left(2\zeta a_0 + \omega_n\right)}{K_{\mathrm{m}}}, \quad (27)$$

$$K_{\mathrm{i,bb}} = \frac{{\omega_n}^2 a_0}{K_{\mathrm{m}}}, \quad (28)$$

$$K_{\mathrm{d,bb}} = \frac{2\zeta\omega_n + a_0}{K_{\mathrm{m}}}, \quad (29)$$

where ω_n is the natural frequency, ζ is the damping ratio *and* a_0 is the pole location.

These parameters decide the third-order system response. After solving under pre-decided specifications, the natural frequency and damping ratio becomes $\omega_n = 2.195\left(\frac{\mathrm{rad}}{\mathrm{s}}\right)$ and $\zeta = 0.638$.

Controller Gains

To meet the criteria, PD and PID controller gains are estimated. In case of the PID controller, the decay time constant (T_a) is considered as 1 s. Controller's gains and other parameters are shown in Table 1.

Steady-State Error

2DBB system x-axis' error can be defined as

$$E(S) = R_{\mathrm{d}}(s) - R(s) \quad (30)$$

From Eq. (24), closed-loop PID response is formulated as

$$R(s) = \frac{K_{\mathrm{m}}\left(s^2 K_{\mathrm{d,bb}} V_{\mathrm{sw}} + sK_{\mathrm{p,bb}} + K_{\mathrm{i,bb}}\right)}{s^3 + s^2 K_{\mathrm{m}} K_{\mathrm{d,bb}} + sK_{\mathrm{m}} K_{\mathrm{p,bb}} + K_{\mathrm{m}} K_{\mathrm{i,bb}}} R_{\mathrm{d}}(s) \quad (31)$$

Substituting Eq. (31) in Eq. (30), the error transfer function of PID is

$$E(s) = \frac{s^2\left(s + K_{\mathrm{m}} K_{\mathrm{d,bb}} - K_{\mathrm{m}} K_{\mathrm{d,bb}} V_{\mathrm{sw}}\right)}{s^3 + s^2 K_{\mathrm{m}} K_{\mathrm{d,bb}} + sK_{\mathrm{m}} K_{\mathrm{p,bb}} + K_{\mathrm{m}} K_{\mathrm{i,bb}}} R_{\mathrm{d}}(s). \quad (32)$$

If $K_{i,bb} = 0$, the error transfer function of PD is

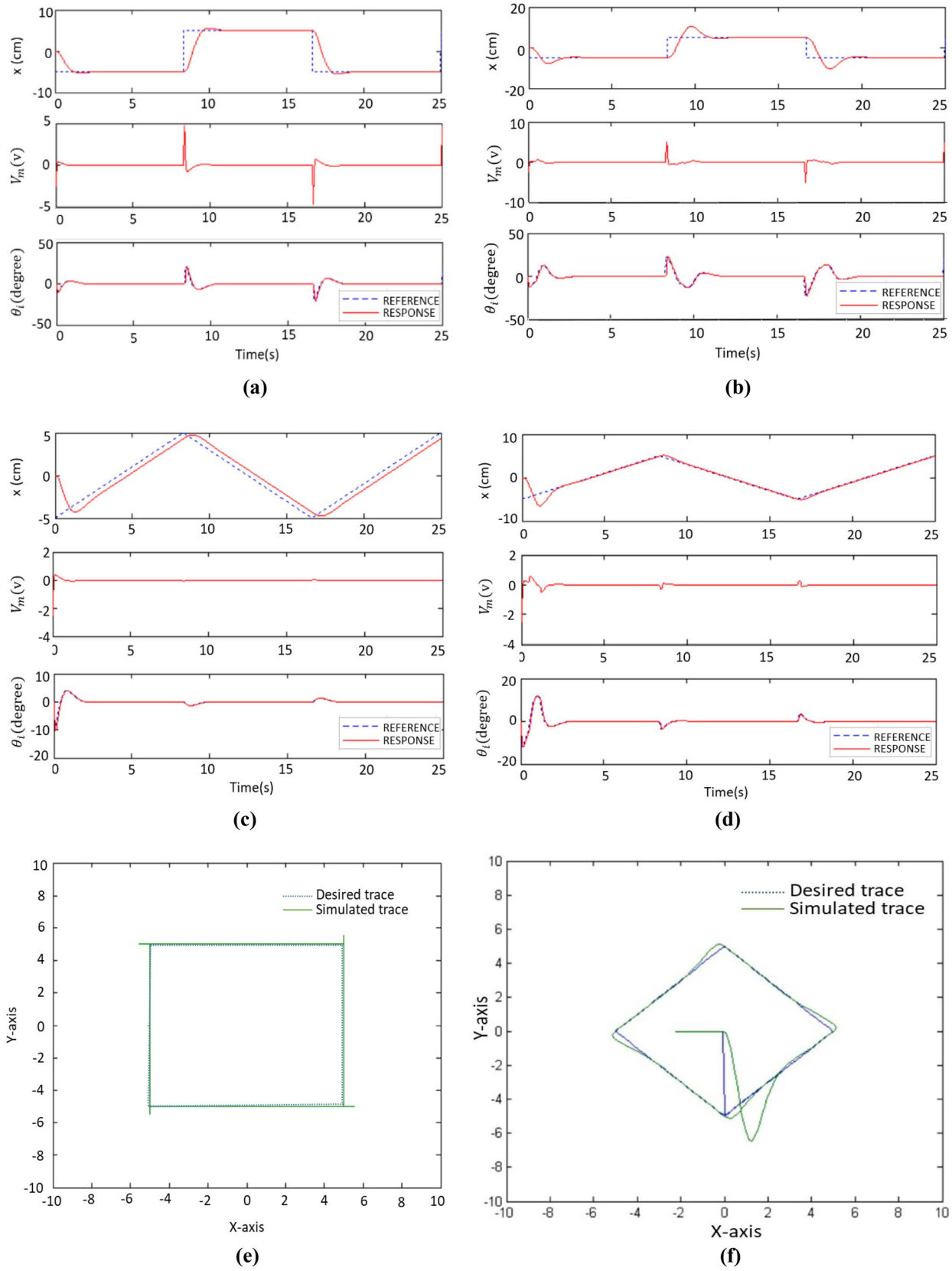

Fig. 9 **a** Step PD response with $V_{sw} = 0$. **b** Step PD response with $V_{sw} = 0.87$. **c** Ramp PD response with $V_{sw} = 0$. **d** Ramp PD response with $V_{sw} = 0.87$. **e** X–Y figure on scope with $V_{sw} = 0$. **f** X–Y figure on scope with $V_{sw} = 0.87$

$$E(s) = \frac{s\left(s + K_{\mathrm{m}}K_{\mathrm{d,bb}} - K_{\mathrm{m}}K_{\mathrm{d,bb}}V_{\mathrm{sw}}\right)}{s^2 + sK_{\mathrm{m}}K_{\mathrm{d,bb}} + sK_{\mathrm{m}}K_{\mathrm{p,bb}}}R_d(s). \tag{33}$$

If a step reference with amplitude a_0 is applied to the error transfer function of PD, then the steady-state error (e_{ss}) will be zero, which is less than the required specification of 0.1 mm. Considering a ramp reference with slope $a_0 = 0.012\left(\frac{m}{s}\right)$ and $V_{\mathrm{sw}} = 0$ is applied to the error transfer function of PD, then e_{ss}=0.7, which is more than the required specification. To meet the specification of e_{ss}<0.1 mm, it is required to design the velocity setpoint weight (V_{sw}).

The steady-state error of PD, when a ramp reference with slope a_0 is applied,

$$e_{\mathrm{ss}} = \frac{a_0K_{\mathrm{d,bb}}\left(V_{\mathrm{sw}} - 1\right)}{K_{\mathrm{p,bb}}}. \tag{34}$$

From this, the mathematics are given as

$$V_{\mathrm{sw}} = \frac{a_0K_{\mathrm{d,bb}} - K_{\mathrm{p,bb}}.e_{\mathrm{ss}}}{a_0K_{\mathrm{d,bb}}}. \tag{35}$$

Substituting the steady-state specifications, PD gains and constant values, the required weight setpoint is obtained as 0.863.

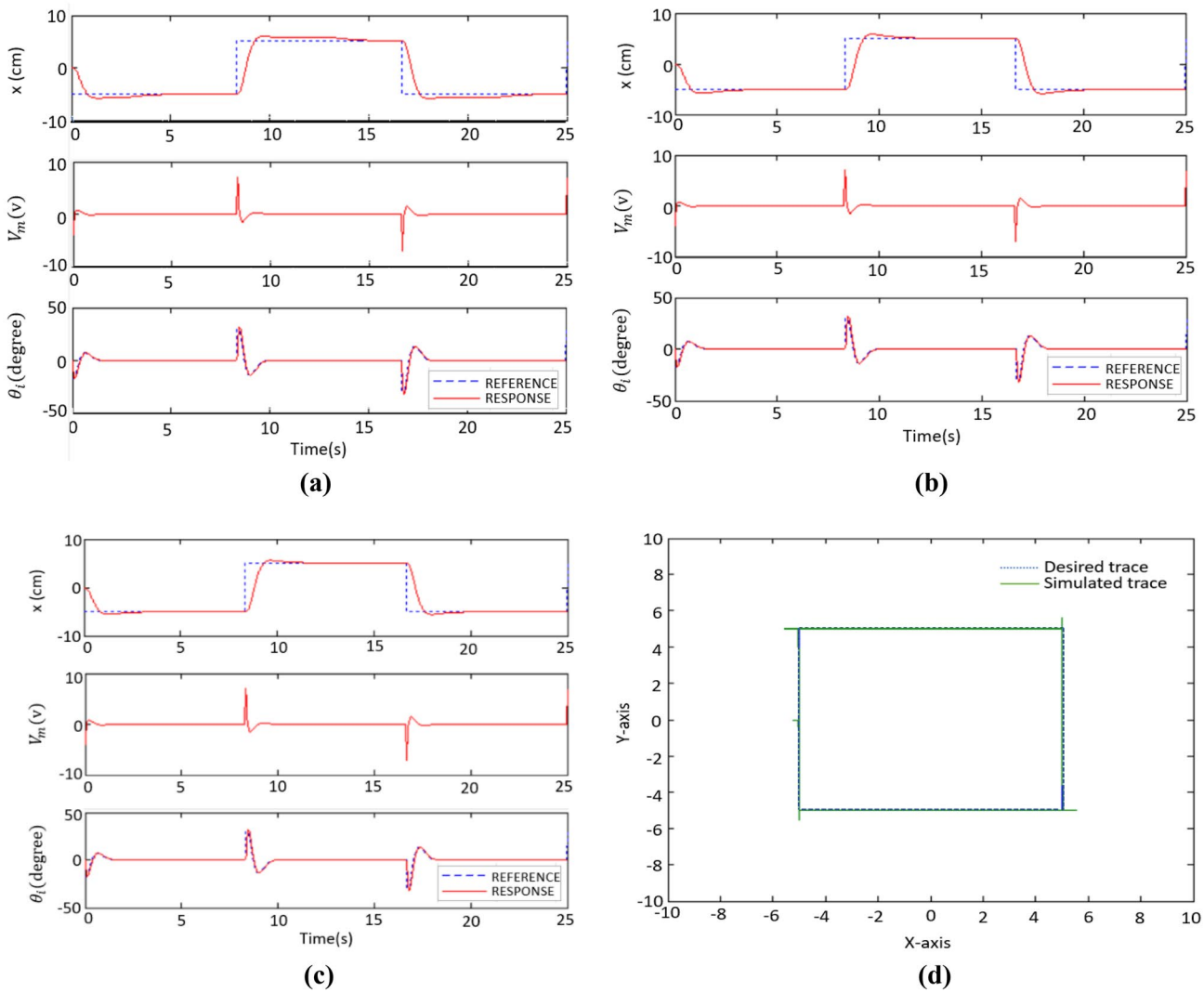

Fig. 10 **a** $\mathrm{INTG_{MAX}} = 2.5$ deg, $T_{\mathrm{aw}} = 5s$. **b** $\mathrm{INTG_{MAX}} = 2.5$ deg, $T_{\mathrm{aw}} = 0.001s$. **c** $\mathrm{INTG_{MAX}} = 1.6$ deg, $T_{\mathrm{aw}} = 0.001s$. **d** X–Y figure on scope with $\mathrm{INTG_{MAX}} = 1.6$ deg, $T_{\mathrm{aw}} = 0.001s$ and $V_{\mathrm{sw}} = 0$

Table 2 Comparison of the outputs of the PD and PID simulations

S. no.	Parameters → Desciption↓	Peak overshoot (PO) %	Settling time (t_s)s	Steady-state error (e_{ss}) cm
1	Step PD response with $V_{sw} = 0$, Fig. 9a	5.62	2.39	0
2	Step PD response with $V_{sw} = 0.87$, Fig. 9b	51.7	2.501	0
3	Step PID response with $V_{sw} = 0$, $\text{INTG}_{\text{MAX}} = 2.5$ deg, $T_{aw} = 5s$, Fig. 10a	8.12	6.1	0.0149
4	Step PID response with $V_{sw} = 0$, $\text{INTG}_{\text{MAX}} = 2.5$ deg, $T_{aw} = 0.001s$, Fig. 10b	7.4	2.45	0.0086
5	Step PID response with $V_{sw} = 0$, $\text{INTG}_{\text{MAX}} = 1.6$ deg,$T_{aw} = 0.001s$, Fig. 10c	5.46	2.28	0.000119

PID with Integral ANTI-WINDUP

When the control system includes an integrator, the actuator limits should be taken into consideration. This limitation is due to the amplifier's maximum supply voltage, which is the inherent capability of the actuator. When the actuator gets saturated by the controller, maybe due to large setpoint, the integrator keeps on increasing to compensate for the error. This process is called integral windup. As a result, the system has large overshoots and becomes unstable. The integral term in the PID controller makes the output to change continuously until there is zero error. But sometimes error cannot be eliminated quickly and within a particular time frame, larger and larger integral terms are produced and continues to happen until saturation is achieved. This is termed as integral windup. This leads to the system's bad performance in terms of peak overshoot. That is why, instead of a simple PID compensator, only PID with Integral ANTI-WINDUP technique is implemented over the ball balancer system for simulation and real-time experimentation to reduce these unnecessary oscillations.

Figure 7 shows the design of the PID controller with Integral ANTI-WINDUP. Contrary to the traditional PID controller, this design includes another loop around the integrator. In case of integrator saturation, this additional loop prevents it from building up too much intensity by decreasing the integrator input. The integrator is designed to saturate at parameter INTG_{MAX}.

The integral control action is defined as

$$m_i = \left\{ \begin{array}{c} -\text{INTG}_{\text{MAX}} n_i < -\text{INTG}_{\text{MAX}} \\ n_i n_i < -\text{INTG}_{\text{MAX}} < 0 and - \text{INTG}_{\text{MAX}} - n_i < 0 \\ \text{INTG}_{\text{MAX}} < n_i \end{array} \right\} \tag{36}$$

where INTG_{MAX} is the upper limit of the integrator. T_{aw} represents the time constant of the anti-windup loop and activates only when the integrator saturates. The integrator reset time depends on T_{aw}. When m_i=n_i, then the integrator is in normal control action. But in case of integration saturation, the anti-windup controller makes the saturation error zero and the iIntegrator output re aches saturation limits, i.e. INTG_{MAX} and $-\text{INTG}_{\text{MAX}}$.

Tracking Ball Position via a Camera

The overhead camera visible in Fig. 1b tracks the ball's position and controllers predict the precise position and provide the planar position of the ball as an output. The viewing area is considered to be a square by making the resolutions (res) of the x-axis and y-axis equal. To track the position along the height (elevation) and width, the x-axis and y-axis pixels are represented as P_{ix} and P_{iy}, respectively, and in the coordinate system, represented as $[X_{\text{co}}, Y_{\text{co}}]$ as shown in Fig. 8.

The functions describing the ball position from camera pixels P_{ix} and P_{iy} relatively to ball coordinates $[X_{\text{ball}}, Y_{\text{ball}}]$ are x and y and can be expressed as

$$x = \left\{ \frac{P_{ix}}{\text{res}} - 0.5 \right\} l_t, y = \left\{ \frac{P_{iy}}{\text{res}} - 0.5 \right\} l_t, \tag{37}$$

where l_t represents the table length.

Results and Discussion

The 2D ball balancer system's closed-loop response is initially simulated using proportional–derivative (PD) and proportional–integral–derivative (PID) controllers with

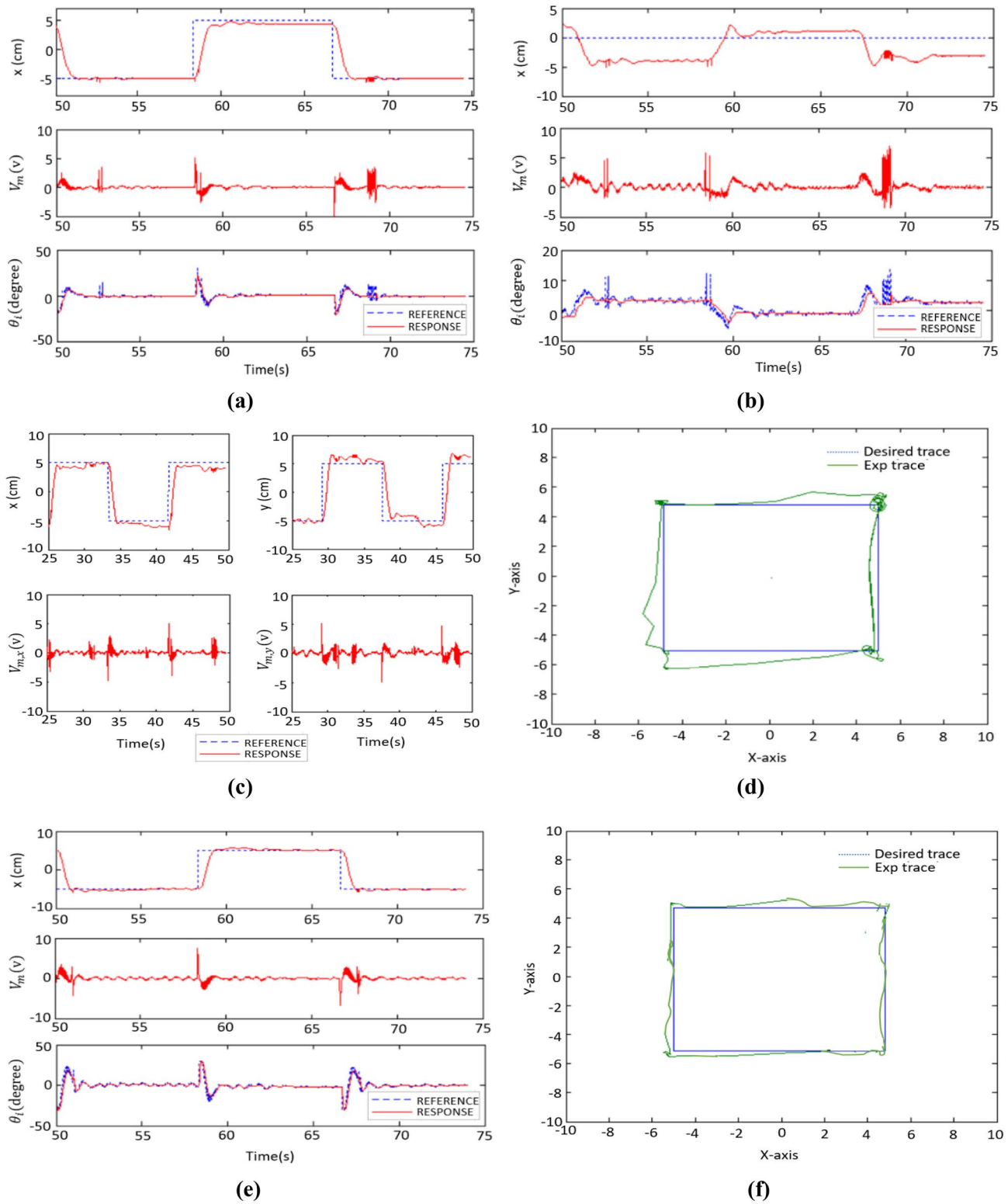

Fig. 11 **a** PD step response along the *x*-axis. **b** PD step response along the y-axis. **c** PD step dual axis response. **d** X–Y figure on scope with $V_{sw} = 0$. **e** PID step response along the *x*-axis. **f** X–Y figure on scope with $V_{sw} = 0$

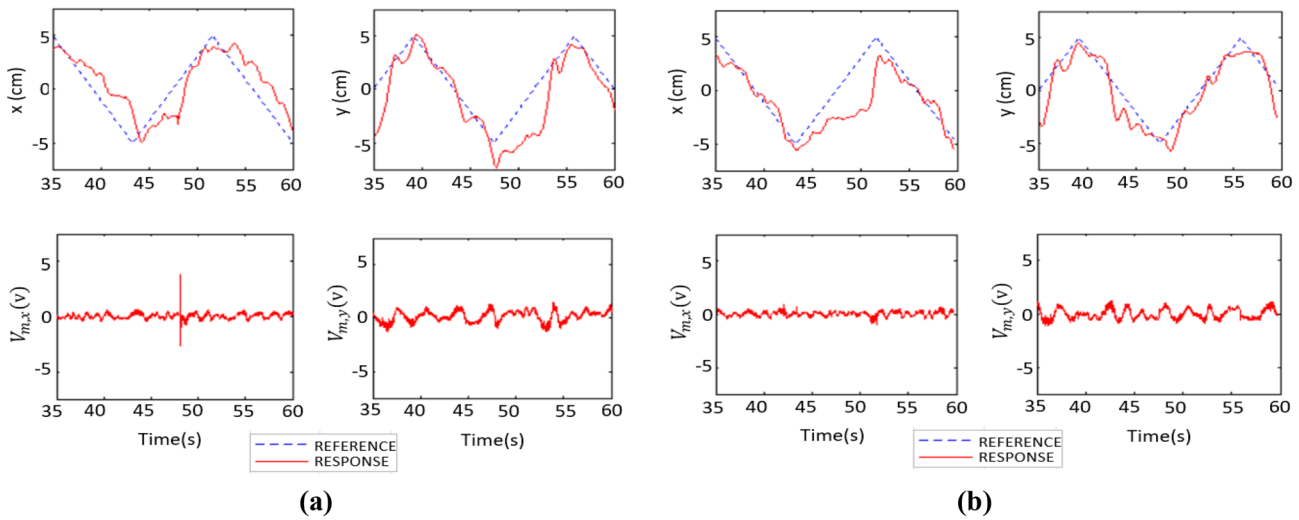

Fig. 12 **a** PD Ramp response with $V_{sw} = 0$. **b** PD ramp response with $V_{sw} = 0.87$

different velocity setpoint weights (V_{sw}) and with different kind of inputs like step input, ramp input and sinusoidal input. After that, real-time experimentation was carried out on hardware setup, shown in Fig. 1b. The closed- loop responses show the signatures of the input servo motor voltage V_m(v), controlled output ball position x (cm) and servo load gear angle θ_i(degree). The X–Y figures are obtained on scope with respect to different applied inputs and V_{sw} values. For both simulation and experimental or real-time process, direct derivative computation of the ball velocity cannot be obtained because of some inherent noise in the measurement of ball position and if we take derivative of this noise, it would result in the amplification of the high-frequency signal which is being fed to the motor.

Simulation-Based Position Control of the Ball Balancer with PD and PID Controllers

1. Step and ramp PD response: Step and ramp input responses of the PD controller is simulated using different values of V_{sw}, i.e. 0 and 0.87 as shown in Fig. 9a–d, respectively, to verify whether the specifications are met or not. It is noticed that as V_{sw} increases, the peak overshoot increases abruptly, but steady-state error is the same for both values of V_{sw} in case of step input. In case of ramp response, steady-state error is the main concern. It is evident that for increase in the V_{sw} value, there is no major effect on steady-state error. The steady-state error is 0.692 cm and 0.13 cm for V_{sw}= 0 and 0.87, respectively, which is under the required criteria and very close to the theoretical values, for both cases. The X–Y figures obtained in case of step response with $V_{sw} = 0$ and ramp respnse with $V_{sw} = 0.87$ are shown in Fig. 9e and f, respectively. When $V_{sw} = 0$, it is noticed that both the desired trace and simulated trace overlap with each other. But when $V_{sw} = 0.87$ is taken for ramp respnse, there is a little steady-state error in the diamond shaped response which is less than the required specification.
2. Step PID response: While implementing additional integral controller to PD controller, $V_{sw} = 0$ is taken because $V_{sw} = 1$ would create too much oscillations. The PID controller is simulated for $INTG_{MAX} = 2.5$ degrees, anti-windup time constant $T_{aw} = 5s$; $INTG_{MAX} = 2.5$ degrees, $T_{aw} = 0.001s$ and $INTG_{MAX} = 1.6$ degrees, $T_{aw} = 0.001s$ as shown in Fig. 10a–c, respectively. Decreasing anti-windup time results in lesser integral reset time and as a result the integral does not get any windup chance, and the settling time reduces to a great extent as evident in Fig. 10b, c. Decreasing $INTG_{MAX}$ value also reduces peak overshoot. However, the servo angle gets saturated, but it does not create any instability due to proper tuning of the windup control. As a result, there is no saturation to the servo motor. The X–Y figure obtained when $INTG_{MAX} = 1.6$ degrees, $T_{aw} = 0.001s$ and $V_{sw} = 0$, in Fig. 10d, shows almost a perfect square where both the desired and simulated traces overlap after tuned windup. Table 2 shows the comparison of the outputs of the PD and PID simulations.

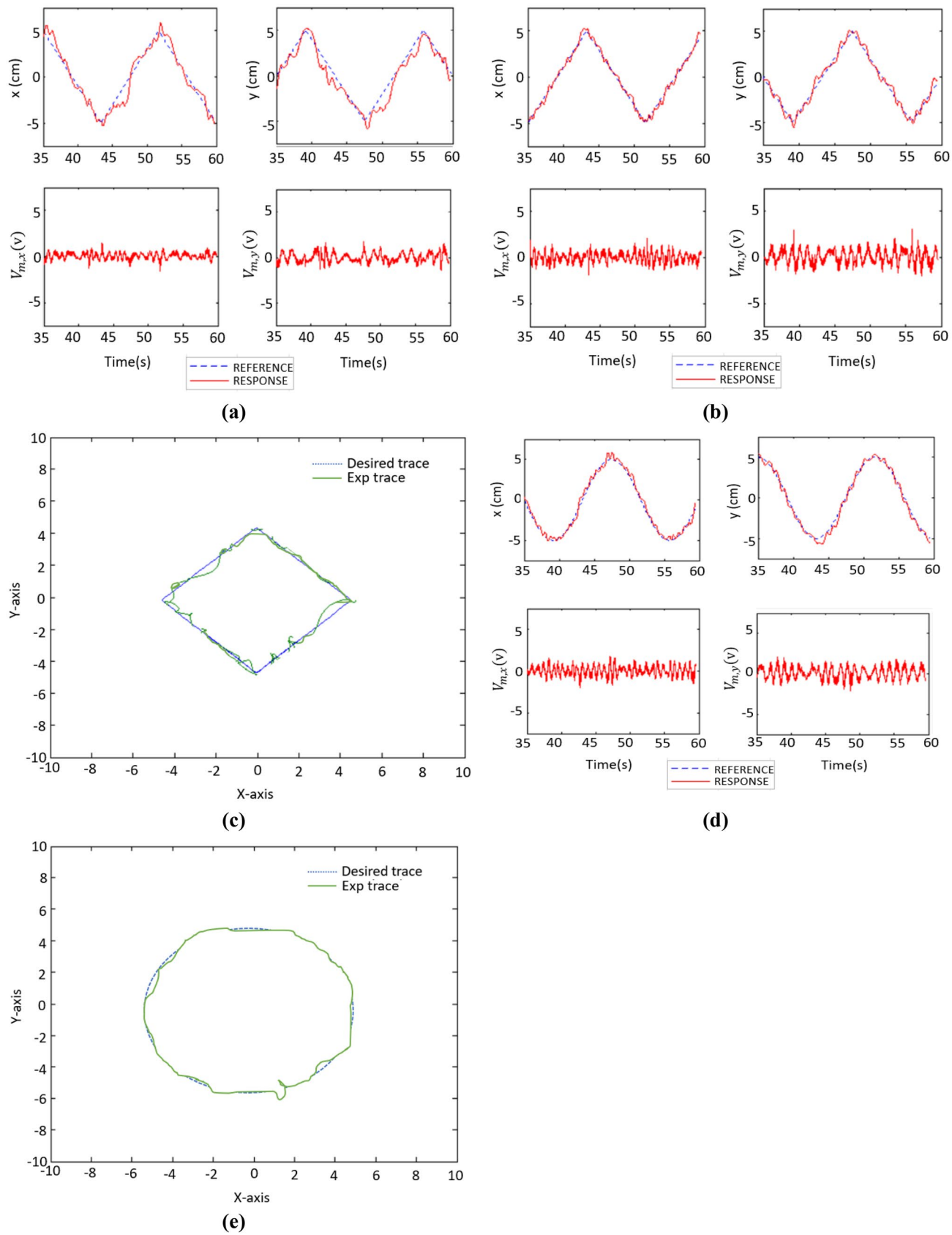

Fig. 13 **a** PID Ramp response with $T_a = 1s$. **b** PID ramp response with $T_a = 0.35s$. **c** X–Y figure on scope with $V_{sw} = 0.87$ and $T_a = 0.35$ s with ramp input. **d** PID sine response with $T_a = 0.35s$. **e** X–Y figure on scope with $V_{sw} = 0.87$ and $T_a = 0.35$ s with sine input

During simulation, the PID compensator provides better results in terms of both transient and steady-state responses. Taking reference of Table 2, step PD response with $V_{sw} = 0$, shown in Fig. 9a, gives peak overshoot (PO%) as 5.62 and settling time as 2.39 s, whereas the step PID response with $V_{sw} = 0, \text{INTG}_{MAX} = 1.6$ deg, $T_{aw} = 0.001s$, shown in Fig. 10c, gives peak overshoot (PO%) as 5.46 and settling time as 2.28 s. The steady-state error is also negligible in case of the PID compensator.

Real-Time Experimentation-Based Position Control of Ball Balancer with PD and PID Controllers

(1) Step PD response along the -*x* and *y*-axis: PD step responses along the *x*- and *y*-axis are shown in Fig. 11a and b. Along the *x*-axis, t_s is1.13 s, PO is 5.11% and e_{ss} is 0.61 cm, which do not meet the requirements. While measuring the response along the *y*-axis, the setpoint is chosen only in the *x*-direction. But it is noticed that the *y*-axis servo also performs a control action. This is due to the coupling difference between both axes. When the *x*-axis servo tries to control the ball position along the *x*-axis, the plate angle in the *y*-direction also changes. Now the ball has to track the step inputs in both the *x*- and *y*-directions simultaneously. The PD step dual axis response is shown in Fig. 11c. $V_{m,x}$ and $V_{m,y}$ show the input servo motor voltage along the *x*- and *y*-axis, respectively, and similarly, *x* (cm) and *y* (cm) show the controlled output ball position along the height and width, respectively. Evidently, each axis causes disturbances on the other axis while tracking the setpoint. The X–Y figure obtained on scope shows the PD response in Fig. 11d, which is not a perfect square due to large steady-state error.

(2) PID step response: PID step response with $V_{sw} = 0$, $\text{INTG}_{MAX} = 1.6$ deg, $T_{aw} = 0.001$ s is shown in Fig. 11e. PO is 5.65% and $e_{ss} = 0.082$ cm. The steady-state error is hugely improved while using the PID controller. The X–Y figure obtained on scope, shown in Fig. 11f, also shows a better response while using PID controller as compared to PD controller.

(3) PD ramp response: Dual axis PD ramp responses with $V_{sw} = 0$ *and* $V_{sw} = 0.87$ are shown in Fig. 12a and b. $V_{m,x}$ and $V_{m,y}$ show the input servo motor voltage along the *x*- and *y*-axis, respectively, and similarly, *x* (cm) and *y* (cm) show the controlled output ball position along the height and width, respectively. However, by varying V_{sw} also, the responses are quite similar. This is because, unmodelled effects like cross-axis coupling and friction have a much bigger effect on the response.

(4) Ramp and sinusoidal PID response: Dual axis PID ramp response with $V_{sw} = 0.87$ and $T_a = 1$ s is shown in Fig. 13a. It is observed that the control effort required to track a ramp input is much lesser than in case of step input. So, T_a needs to be tuned accordingly to get a better response. Dual axis PID ramp response with $V_{sw} = 0.87$ and $T_a = 0.35$ s is shown in Fig. 13b. This shifts the desired pole location more towards the left side of the plane and thus controller gain values increase. Updated controller gains are $K_{p,bb} = 14.2\text{rad/m}, K_{i,bb} = 18.9$ rad/m. s, $K_{d,bb} = 5.987$ rad. s/m. $V_{m,x}$ and $V_{m,y}$ show the input servo motor voltage along the *x*- and *y*-axis, respectively, and similarly, *x* (cm) and *y* (cm) show the controlled output ball position along the height and width, respectively. The X–Y figure obtained on scope, corresponding to PID ramp input for $T_a = 0.35$ s and $V_{sw} = 0.87$, is shown in Fig. 13c. For the same controller values, dual axis PID sinusoidal response with $V_{sw} = 0.87$ and $T_a = 0.35$ s is shown in Fig. 13d. The X–Y figure obtained on scope, corresponding to PID sinusoidal response for $T_a = 0.35$ s and $V_{sw} = 0.87$, is shown in Fig. 13e. With decrease in T_a values, the responses are far better than previously.

During real-time experimentation, for step PD response along x, e_{ss} is 0.61 cm which does not meet the requirements. But in case of PID step response, e_{ss} is 0.082 cm, which is hugely improved as compared to the step PD response. PID square response in Fig. 11f is smoother than the PD square response in Fig. 11d. Also, the trajectories of ramp PID responses in Fig. 13a, b are much smoother than the PD ramp responses in Fig. 12a, b. All these observations make the PID compensator better than the PD compensator.

Conclusion

The work illustrated the modelling of the 2-DOF ball balancer system, implementation of various controllers like PD, PID and PID with Integral ANTI-WINDUP with different velocity setpoint (V_{sw}) and comparison of these implemented controllers on the system. The outcomes of the system for these controllers are demonstrated on the basis of simulation and real-time experimentation results. Peak overshoot, settling time and steady-state error analysis were carried out for these controllers. The outcomes of simulation and experimental assessment implies that PID with Integral ANTI-WINDUP controller has overall better control performances for the ball balancer system.

The PID controller showed a better performance because of its ability to reduce the steady-state error that occurs between the reference and generated output. For future prospect, relatively more advanced hybrid control strategies such as type 2 NiF-PID, wavelet NiF-PID, along with optimiszation algorithms can be implemented for control. Much more extensive analysis may be carried out for robustness analysis, thus allowing the system to withstand against external disturbances. The SRV02 unit may also be investigated further for performing vibration analysis of the system.

Author Contributions All authors read and approved the final manuscript.

Funding The authors received no specific funding for this study.

Data Availability The datasets used and/or analysed during the current study available from the corresponding author on reasonable request.

Code Availability Code is available.

Declarations

Conflict of Interest On behalf of all authors, the corresponding author states that there is no conflict of interest.

References

1. Bars R et al (2006) Theory, algorithms, and technology in the design of control systems. Annu Rev Control 30(1):19–30
2. Murray R (2003) Future directions in control, dynamics, and systems: overview, grand challenges, and new courses. Eur J Control 9(2–3):144–158
3. Kheddar A, Caron S, Gergondet P, Comport A, Tanguy A, Ott C, Henze B, Mesesan G, Englsberger J, Roa MA, Wieber PB (2019) Humanoid robots in aircraft manufacturing: the airbus use cases. IEEE Robot Autom Mag 26(4):30–45
4. Wang Y, Zhu Q, Xiong R, Chu J (2013) Standing balance control for position control-based humanoid robot. IFAC Proc Vol 46(20):429–436
5. Patle BK, Pandey A, Parhi DRK, Jagadeesh A (2019) A review: on path planning strategies for navigation of mobile robot. Def Technol 15:582–606
6. Zhang B, Zong Q, Dou L, Tian B, Wang D, Zhao X (2019) Trajectory optimization and finite-time control for unmanned helicopters formation. IEEE Access 7:93023–93034
7. Zhao J, Ding X, Jiang B, Jiang G, Xie F (2021) A novel control strategy for quadrotors with variable mass and external disturbance. Int J Robust Nonlinear Control 31(17):8605–8631
8. Liu C, Jiang B, Zhang K, Ding SX (2022) Hierarchical structure-based fault-tolerant tracking control of multiple 3-DOF laboratory helicopters. IEEE Trans Syst, Man, Cybern: Syst 52(7):4247–4258
9. Boubaker O (2012) The inverted pendulum: a fundamental benchmark in control theory and robotics. In: International Conference on Education, e-Learning and Innovations
10. Rigatos G, Siano P, Abbaszadeh M, Ademi S, Melkikh A (2018) Nonlinear H-infinity control for underactuated systems: the Furuta pendulum example. Int J Dyn Control 6:835–847
11. Alves UN, Breganon R, Pivovar LE, de Almeida JP, Barbara GV, Mendonça M, Palácios RH (2022) Discrete-time H∞ integral control via LMIs applied to a Furuta pendulum. J Control, Autom Electr Syst 33(3):1–2
12. Mehedi IM, Al-Saggaf UM, Mansouri R, Bettayeb M (2019) Two degrees of freedom fractional controller design: application to the ball and beam system. Measurement 135:13–22
13. Yan L, Ma B, Xie W (2021) Robust practical tracking control of an underactuated hovercraft. Asian J Control 23(5):2201–2213
14. Ali HI, Jassim HM, Hasan AF (2019) Optimal nonlinear model reference controller design for ball and plate system. Arab J Sci Eng 44(8):6757–6768
15. Rigatos G, Cuccurullo G, Busawon K, Gao Z, Abbaszadeh M (2022) Nonlinear optimal control of the ball and plate dynamical system. AIP Conf Proc. https://doi.org/10.1063/5.0081624
16. Spacek L, Vojtesek J (2018) Overview of ball and plate application for collaborative robot YuMi. In: IEEE International conference on innovation, engineering and entrepreneurship, Springer. pp 89–95
17. Jang H-G, Hyun C-H, Park B-S (2021) Neural network control for trajectory tracking and balancing of a ball-balancing robot with uncertainty. Appl Sci 11(11):4739
18. Elshamy MR, Nabil E, Abdelmageed AS, Abozalam B (2021) Stabilization enhancement of the ball on the plate system (BOPS) based on Takagi-Sugeno (T-S) fuzzy modeling. In: Proceedings of the 2nd IEEE International Conference on Electronic Engineering (ICEEM). pp 3–4
19. Zakeri E, Moezi SA, Eghtesad M (2019) Optimal interval type-2 fuzzy fractional order super twisting algorithm: a second order sliding mode controller for fully-actuated and under-actuated nonlinear systems. ISA Trans 85:13–32
20. Bang H, Lee YS (2018) Implementation of a ball and plate control system using sliding mode control. IEEE Access 6:32401–32408
21. Das A, Roy P (2017) Improved performance of cascaded fractional-order SMC over cascaded SMC for position control of a ball and plate system. IETE J Res 63(2):238–247
22. Bang H, Lee Y (2019) Embedded model predictive control for enhancing tracking performance of a ball-and-plate system. IEEE Access 7:39652–39659
23. Umar A, Mu'azu MB, Usman AD, Musa U, Ajayi OO, Yusuf AM (2019) Linear quadratic Gaussian (LQG) control design for position and trajectory tracking of the ball and plate system. Comput Inf Syst 23(1)
24. Núñez D, Acosta G, Jiménez J (2020) Control of a ball-and-plate system using a state-feedback controller. Ingeniare 28(1):6–15
25. Betancourt FIR, Alarcon SMB, Velasquez LFA (2019) Fuzzy and PID controllers applied to ball and plate system. In: 2019 IEEE 4th Colombian Conference on Automatic Control (CCAC). pp 1–6
26. Oglah AA, Msallam MM (2021) Real-time implementation of fuzzy logic controller based on chicken swarm optimization for the ball and plate system. Int Rev Appl Sci Eng. https://doi.org/10.1556/1848.2021.00360
27. Azar AT, Ali N, Makarem S, Diab MK, Ammar HH (2020) Design and implementation of a ball and beam PID control system based on metaheuristic techniques. In: International Conference on Advanced Intelligent Systems and Informatics (AISI). Advances in Intelligent Systems and Computing. 1058. Springer, Cham
28. Hadoune O, Benouaret M, Zeghida A, Saker H (2021) Tracking control of a ball on plate system using PID controller and Lead/Lag compensator with a double loop feedback scheme. Eur J Sci Technol 11(28):375–380

29. Mohammadi A, Ryu JC (2020) Neural network-based PID compensation for nonlinear systems: ball-on-plate example. Int J Dyn Control 8(1):178–188
30. Zheng L, Hu R (2019) Robust and fast visual tracking for a ball and plate control system: design, implementation and experimental verification. Multimed Tools Appl 78:13279–13295
31. Do VT, Lee SG (2020) Neural integral backstepping hierarchical sliding mode control for a ridable ballbot under uncertainties and input saturation. IEEE Trans Syst, Man, and Cybern: Syst 51(11):7214–7227
32. Ma J, Tao H, Huang J (2021) Observer integrated backstepping control for a ball and plate system. Int J Dyn Control 9:141–148
33. Elshamy MR, Abozalam B, Sayed A, Nabil E (2022) Real-time control design and implementation of ball balancer system based on machine learning and machine vision. Concurr Comput: Pract Exp 34(27):e7317
34. Jang HG, Hyun CH, Park BS (2023) Virtual angle-based adaptive control for trajectory tracking and balancing of ball-balancing robots without velocity measurements. Int J Adapt Control Signal Process 37(8):2204–2215
35. OkaforE UD, Ibrahim Y, Mu'azu MB, Okafor EG (2021) Heuristic and deep reinforcement learning-based PID control of trajectory tracking in a ball-and-plate system. J Inf Telecommun 5(2):179–196
36. Haddad F, Tamimi J (2023) A comparative simulation and experimental study for control of a ball and plate system using model-based controllers. Int J Dyn Syst Differ Equ 13(2):91–107
37. Zaare S, Soltanpour MR (2021) The position control of the ball and beam system using state-disturbance observe-based adaptive fuzzy sliding mode control in presence of matched and mismatched uncertainties. Mech Syst Signal Process 150:107243
38. Li JF, Xiang FH (2022) RBF network adaptive sliding mode control of ball and plate system based on reaching law. Arab J Sci Eng 47:9393–9404
39 Khaled N, Pattel B, Siddiqui A (2020) Digital twin development and deployment on the cloud: developing cloud-friendly dynamic models using Simulink®/Simscape™ and Amazon AWS. Academic Press
40. Ker CC, Lin CE, Wang RT (2007) Tracking and balance control of ball and plate system. J Chin Inst Eng Trans 30(3):459–470
41. Quanser Inc (2010) Peripherals to accelerate control system design and implementation. 12
42. Escobar LM, Gordón M, Quintero OC, Rosales A, Pozo D (2017) A comparative analysis among different controllers applied to the experimental ball and plate system. In: 2017 IEEE International Conference on Information Systems and Computer Science (INCISCOS). pp 108–114
43. Electronics M. Faulhaber DC-Micromotors Series 2338